Acta Cryst. (1995). B**51**, 688–697

The Structure Refinement of Compositely Modulated $Nb_2Zr_{x-2}O_{2x+1}$ ($x = 12$)

BY KLAUS FÜTTERER, SIEGBERT SCHMID, JOHN G. THOMPSON AND RAY L. WITHERS*

Research School of Chemistry, Australian National University, Canberra ACT 0200, *Australia*

NOBUO ISHIZAWA

Research Laboratory of Engineering Materials, Tokyo Institute of Technology, Nagatsuta, Midori-ku, Yokohama 226, *Japan*

AND SHUNJI KISHIMOTO

National Laboratory for High Energy Physics, Oho, Tsukuba 305, *Japan*

(*Received* 11 *November* 1994; *accepted* 9 *December* 1994)

Abstract

The room-temperature single-crystal X-ray structure refinement of $Nb_2Zr_{x-2}O_{2x+1}$, $x = 12$, as an incommensurate compositely modulated structure is reported. It consists of two component substructures, referred to as the metal substructure (M), $a_M = 5.108(1)$, $b_M = 4.997(1)$, $c_M = 5.278(1)$ Å, and the oxygen substructure (O), $a_O = 2.452$ Å, $b_O = b_M = b$, $c_O = c_M = c$, respectively. The primary modulation wavevector of the M substructure is chosen to be $\mathbf{q}_M = \mathbf{a}_O^* - 2\mathbf{a}_M^* + \mathbf{b}^* = 1/12\mathbf{a}_M^* + \mathbf{b}^*$. The overall superspace group symmetry is $Amma(\alpha 10)0s0$. Two sets of intensity data, recorded 8 ($\lambda_1 = 0.6892$ Å) and 1458 eV ($\lambda_2 = 0.7495$ Å) below the Zr K absorption edge, were refined to an overall $wR(\lambda_1) = 0.0406$ and $wR(\lambda_2) = 0.0687$. The displacive modulation wave amplitudes obtained from these refinements are in remarkable agreement with those obtained from a Fourier decomposition of the previously published, conventional superstructure refinement of the member $x = 8$ [Galy & Roth (1973). *J. Solid State Chem.* **7**, 277–285]. Despite the enhanced scattering contrast between Zr and Nb at λ_1, metal-ion ordering was not found to be significant. Comparative refinements as incommensurately and commensurately modulated structures gave distinctly better R-values for the former case.

1. Introduction

The structures of solid solutions in 'stabilized' zirconia systems have attracted considerable attention from both solid-state chemists and crystallographers for many years (Roth, Waring, Brower & Parker, 1972; Makovicky & Hyde, 1981, and references therein; Eyring, 1979). These structures have the ability to adapt continuously over an often extraordinarily wide anion-to-cation composition range, while maintaining the essential integrity of both their *fcc* cation array and the structure type, as measured by the absence of two-phase regions. Both anion-deficient and anion-excess ZrO_2-containing oxides behave in this manner. Detailed crystallographic and crystal chemical understanding, however, is often still lacking. This contribution focuses on one such anion-excess system.

At the ZrO_2-rich end of the $ZrO_2.Nb_2O_5$ system, a wide-range $Nb_2Zr_{x-2}O_{2x+1}$ solid solution is observed. The width of this solid solution, when synthesized *via* solid-state reaction, has been reported as $7.1 \leq x \leq 10.3$ (Thompson, Withers, Sellar, Barlow & Hyde, 1990). In the present investigation x is beyond the range previously reported, but this is attributed to the synthesis being carried out *via* a flux method (see §2.1). While Roth *et al.* (1972) considered this composition field to be made up of a homologous series M_nO_{2n+1} ($x = 2n$) of closely related phases, Thompson *et al.* (1990) have shown that the description of the $Nb_2Zr_{x-2}O_{2x+1}$ system as a composite modulated structure is more appropriate.

This latter approach describes the structure of any particular member of the solid solution in terms of two mutually incommensurable parent substructures (a metal atom or M substructure and an oxygen atom or O substructure) and atomic modulation functions [AMF's (Withers, Thompson & Hyde, 1991)] describing the deviation of atomic positions from their respective positions in the underlying parent substructures. The primary modulation wavevector characteristic of these AMF's is determined by the relative periodicity of the parent substructures and was found to be given by $\mathbf{q}_M = (1/x)\mathbf{a}_M^* + \mathbf{b}_M^*$ (Thompson *et al.*, 1990). Such an approach allows the direct structural comparison of AMF's associated with differing values of x.

To date, only one single-crystal structure refinement of a member of this solid solution has been reported. This

* Author to whom correspondence should be addressed.

was of $Nb_2Zr_6O_{17}$, corresponding to $x = 8$ (Galy & Roth, 1973), and was solved in terms of a conventional superstructure approach. There has, however, also been an unpublished structure refinement of the $x = 10$ member of the closely related $Ta_2Zr_{x-2}O_{2x+1}$ solid solution, *i.e.* $Ta_2Zr_8O_{21}$ (Galy, 1980). This has been reported in the form of a figure (Fig. 30) in Makovicky & Hyde (1981), showing Ta/Zr ordering and, by analogy, suggests that metal-ion ordering should also occur in the $Nb_2Zr_{x-2}O_{2x+1}$ system. According to this figure, the Ta and (analogously) Nb atoms are situated at so-called antiphase boundaries, where the oxygen array transforms from a square net to a denser packed hexagonal net [see Fig. 6(*b*)]. Due to the low scattering contrast between Zr and Nb when using Mo $K\alpha$ radiation, Galy & Roth (1973) were not able to distinguish between these two elements in their investigation of $Nb_2Zr_6O_{17}$. Therefore, direct experimental evidence for the presence or non-presence of metal-ion ordering in $Nb_2Zr_{x-2}O_{2x+1}$ is still missing.

The purpose of the present paper is to examine whether:

(i) The AMF's describing the structural deviation of the *M* and O substructures from their underlying parent substructures are essentially the same across the whole $Nb_2Zr_{x-2}O_{2x+1}$ solid solution field, *i.e.* whether all occurring structures can be regarded as being equivalent from the 'higher-dimensional' viewpoint of a composite crystal.

(ii) Nb/Zr metal-atom ordering can be detected in such structures, when measuring at an appropriately chosen synchrotron radiation wavelength, in order to enhance the Zr/Nb scattering contrast.

2. Experimental

2.1. *Synthesis*

Single crystals of $Nb_2Zr_{x-2}O_{2x+1}$ were grown using a BaO–V_2O_5 eutectic flux. ZrO_2 and Nb_2O_5 were mechanically mixed in a ratio of 4:1 and the resulting mixture with the flux material (ratio 2.5:1 flux:reactants) heated to 1473 K. The mixture was cooled to 1073 K within 5 d and then quickly to room temperature. Upon dissolving the flux, clear, pale yellow plates of $Nb_2Zr_{x-2}O_{2x+1}$, with $x = 12$, were left. Variation in the ratio between the reactants (range 4:1–7:1) and also between reactants and flux did not change the apparent magnitude of x. This is not consistent with the reported results of Galy & Roth (1973). The value $x = 12$ is outside the range described by Thompson *et al.* (1990), however, their composition range $x = 7.1$–10.3 resulted from solid-state reaction of component oxides. The crystal chosen for intensity measurements approximated a square prism of dimensions $25 \times 25 \times 20\,\mu m^3$ ($= 1.25 \times 10^4\,\mu m^3$).

2.2. *Intensity measurement*

Preliminary tests of crystal quality – magnitude of the wavevector and reflection profiles – were performed on a Rigaku AFC-6*R* four-circle diffractometer with rotating Cu anode. The crystals were mounted on tapered glass fibers with the diameter of the fiber ends being of approximately the same size as the crystals.

The intensity data measurement was carried out using synchrotron radiation on the four-circle diffractometer at vertical wiggler port BL-14A at the Photon Factory (Satow & Iitaka, 1989). In order to determine precisely the location of the Zr *K* absorption edge prior to intensity data collection, a near-edge absorption spectrum of ZrO_2 powder was recorded. The location of the Zr absorption edge was used to provide a calibration of the indicated monochromator position with the absolute incident energy. The precision of this value is limited by the width of the absorption edge, which spans several eV in our experimental data. The edge was defined as the monochromator position that roughly corresponded to the point where absorption had risen half way to its far edge value. All other settings of the incident X-ray energy were defined relative to this value.

Intensity data were recorded at two different wavelengths (1458 and 8 eV below the Zr *K* absorption edge, respectively). The relevant parameters of the data collection are given in Table 1. To improve the counting statistics on weaker reflections, scans were repeated when $\sigma(F)/F$ was larger than 0.05, $\sigma(F)$ being calculated from counting statistics only. The maximum number of scans was 3. Decay of the incident beam and spontaneous fluctuations were monitored with an ion chamber to enable normalization of the raw counts. There was no significant change in intensity once the data had been corrected for the variation of the incident beam resulting from decay of the synchrotron ring current.

No polarization correction was applied as the beam was assumed to be perfectly polarized in the vertical plane, whereas all diffraction (monochromator crystals and four-circle diffractometer) occurred in the horizontal plane. Symmetry equivalent reflections were averaged in the Laue group *mmm* and the merge statistics (see Table 2) indicated no inconsistency with that diffraction symmetry.

2.3. *Data processing*

During the early stages of the refinement, we became aware that a substantial broadening of the satellite reflections compared with the metal parent reflections, which was observed when recording peak profiles on the synchrotron, was relevant for the fit of the model. This broadening is due to an observation made by Thompson *et al.* (1990) that rows of satellite reflections in certain electron diffraction patterns were often slightly canted away from the $\mathbf{a}_M^*$ direction of the metal atom substructure, implying that the irrational component of

Table 1. *Parameters of intensity data collection*

Diffractometer	Single detector, four-circle diffractometer at vertical wiggler port BL-14A, Photon Factory			
Radiation (Å)	$\lambda_2 = 0.7495(4)$		$\lambda_1 = 0.6892(4)$	
Energy difference to Zr K edge (eV)	1458		8	
Monochromator	Si(111) double crystal monochromator			
$\Delta f'$, $\Delta f''$ Zr	−2.045	0.617	−6.866	0.529
Nb	−1.656	0.685	−2.413	0.588
O	0.01	0.007	0.01	0.006
Scan mode	$2\theta/\omega$, $\Delta\omega = 0.6°$			
Data collection limits in 2θ(°), $hklm$	$1 \le 2\theta \le 55$ $-7 \le h \le 7$ $-13 \le k \le 9$ $-7 \le l \le 6$ $-6 \le m \le 6$		$1 \le 2\theta \le 40$ $-5 \le h \le 5$ $-10 \le k \le 9$ $-5 \le l \le 5$ $-6 \le m \le 6$	
No. of measured reflections	11 808; 1260 unique; 835 unique & $F \ge 3\sigma(F)$		4928; 420 unique; 230 unique & $F \ge 3\sigma(F)$	
Standards	8 reflections, measured every 100 reflections			
Orientation check	Every 100 reflections			
Lattice parameters (Å)	61.3040(23) = 12 × 5.1087, 4.9973(3), 5.2775(2) determined from 24 reflections, $34 \le 2\theta \le 48°$, at λ_1			
Modulation wavevector	$\mathbf{q}_M = (1/12)\mathbf{a}_M^* + \mathbf{b}^*$			
Lorentz correction	*Xtal*3.0 (Hall & Stewart, 1990)			
Absorption correction	None		None	
Coefficients a_1, a_2 of scan correction (see §2.2)				
$m = 0$	No correction		No correction	
$m = 1$	0.64, 0.80		1.34, 0.59	
$m = 2$	0.95, 0.51		1.46, 0.44	
$m = 3$	0.96, 0.35		1.84, 0.20	
$m = 4$	No correction		No correction	

Table 2. *Relevant parameters of the refinements (resulting parameters presented in this article)*

Label of refinement run	zrf.B		zr8.B1		zr8.B2	
Wavelength (Å)	$\lambda_2 = 0.7495$		$\lambda_1 = 0.6892$			
Energy difference to Zr K edge (eV)	1458		8			
Occupational modulation	None		None		Harmononic approx.	
Modulation wavevector	$\mathbf{q}_M = (1/12)\mathbf{a}_M^* + \mathbf{b}_M^*$ Incommensurate					
Symmetry	*Amma*(α10)0s0					
No. of refined parameters	26		26		28	
No. of unique reflections $F \ge 3\sigma(F)$						
all	796		205		205	
$m = 0$	171		58		58	
$m = 1$	198		54		54	
$m = 2$	201		66		66	
$m = 3$	138		34		34	
$m = 4$	89		14		14	
Weight	$1/\sigma^2$		$1/\sigma^2$		$1/\sigma^2$	
Residuals R, wR (%)						
overall	6.33	6.87	4.70	4.06	4.87	4.18
$m = 0$	3.39	4.51	2.33	2.49	2.63	2.84
$m = 1$	9.28	9.29	10.05	8.58	9.77	8.42
$m = 2$	10.15	9.49	10.18	9.74	9.53	9.42
$m = 3$	20.36	19.60	19.61	19.15	18.46	18.33
$m = 4$	39.19	36.30	34.72	41.45	31.43	37.14
R_{exp} (%)						
overall	1.68				1.86	
$m = 0$	0.67				0.61	
$m = 1$	2.63				3.08	
$m = 2$	2.95				4.12	
$m = 3$	6.62				9.91	
$m = 4$	29.89				20.14	

the primary modulation wavevector $\mathbf{q}_i$ need not necessarily point directly along $\mathbf{a}_M^*$. The extent of the canting, however, was not reproducible and seemed to vary from grain to grain. Electron diffraction patterns of the present flux-grown material showed similar behavior, as can be seen in Fig. 1. In X-ray diffraction-sized crystals variability in this canting results in a broadening of the satellite reflections perpendicular to the $\mathbf{a}^*$-axis. Table 3 shows the full width at half maximum (FWHM) for some selected main and satellite reflections, obtained from step scans using both $\omega/2\theta$ and ω scan techniques. When looking at satellite reflections situated along $\mathbf{a}^*$, these two scan types correspond to scanning along $\mathbf{a}^*$ and across $\mathbf{a}^*$, respectively. The peak half widths of satellite reflections are up to eight times larger in an ω scan (and roughly three times larger in an $\omega/2\theta$ scan) than those of the parent metal substructure reflections, which are remarkably sharp.

A consequence of recording intensities from such crystals using the $\omega/2\theta$ scan technique (see Table 1) is that, for many satellite reflections, the finite receiving slit width results in the reflection being incorrectly counted, *i.e.* the large difference in peak half widths implies that one records different portions of the whole integrated intensity for satellite reflections on the one hand and main reflections on the other. This problem worsens with increasing satellite order and also becomes increasingly relevant for decreasing $\sin\theta/\lambda$. A linear correction to the F_o's derived from a graph of F_o/F_c *versus* $\sin\theta/\lambda$ was therefore applied. Fig. 2 shows graphs of this type for both the parent reflections and the second-order satellites of the 'far-edge' intensity data set. The linear curve fitted to the data is $F_o/F_c = a_1(\sin\theta/\lambda) + a_2$. While the slope a_1 is 0.15 for the parent reflections, it is 0.95 for the satellite reflections. The F_o's were corrected using the equation $F_o' = F_o\ [a_1(\sin\theta/\lambda) + a_2]^{-1}$. The correction was applied separately for satellites with $m = 1$, 2 and 3. No correction was applied to the main reflections and the fourth-order satellites, because the latter showed a large scatter F_o/F_c around 1, resulting in a_1 being almost zero. The correction coefficients are listed in Table 1.

3. Symmetry

The structure refinement of $Nb_2Zr_6O_{17}$ (Galy & Roth, 1973) was studied by Withers *et al.* [(1991) abbreviated in the following as WTH] using a modulation wave approach. Therein the derivation of the symmetry of the whole solid solution was presented in detail. As the present work is based on this earlier paper, the reader is referred to it for further detail. Subsequently, only those facts relevant to the present refinement are summarized.

(i) The $Nb_2Zr_{x-2}O_{2x+1}$ solid solution can be regarded as a (3 + 1)-dimensional composite modulated structure, consisting of two subsystems – a metal ion or M subsystem and an oxygen ion or O subsystem. The lattice parameters for our $x = 12$ specimen are (see Table 1 for

Table 3. *Scan widths*

hklm	FWHM (°)	Scan type
2000	0.064	$\omega/2\theta$
4000	0.065	$\omega/2\theta$
6000	0.067	$\omega/2\theta$
$220\bar{5}$	0.205	$\omega/2\theta$
$2\bar{2}02$	0.201	$\omega/2\theta$
$420\bar{5}$	0.185	$\omega/2\theta$
$4\bar{2}02$	0.160	$\omega/2\theta$
$620\bar{5}$	0.177	$\omega/2\theta$
$6\bar{2}02$	0.141	$\omega/2\theta$
0001	0.190	$\omega/2\theta$
$2\bar{2}02$	0.187	$\omega/2\theta$
2111	0.171	$\omega/2\theta$
4000	0.065	$\omega/2\theta$
0001	0.535	ω
$2\bar{2}02$	0.393	ω
2111	0.304	ω
4000	0.066	ω

standard deviations)

M: $a_M = 5.108$, $b_M = 4.997$, $c_M = 5.278$ Å
O: $a_O = [x/(2x+1)]$, $a_M = 2.452$ Å, $b_O = b_M$, $c_O = c_M$.

Since b and c are identical for both subsystems, the indices for those two axes are omitted.

(ii) Following WTH, the primary modulation wavevector of the metal subsystem is chosen to be

$$\mathbf{q}_M = (110)^*_O - (200)^*_M = \mathbf{a}^*_O - 2\mathbf{a}^*_M + \mathbf{b}^* = (1/x)\mathbf{a}^*_M + \mathbf{b}^*,$$

whereas the primary modulation wavevector of the oxygen subsystem is chosen to be $\mathbf{q}_O = \mathbf{a}^*_M$.

(iii) The matrix W (see van Smaalen, 1991), transforming the metal ion subsystem into the oxygen ion subsystem is given by

$$W = \begin{pmatrix} 2 & -1 & 0 & 1 \\ 0 & 1 & 0 & 0 \\ 0 & 0 & 1 & 0 \\ 1 & 0 & 0 & 0 \end{pmatrix},$$

with $(\mathbf{a}^*, \mathbf{b}^*, \mathbf{c}^*, \mathbf{q})_O = (\mathbf{a}^*, \mathbf{b}^*, \mathbf{c}^*, \mathbf{q})_M\ W^T$, where W^T is the transposed matrix.

(iv) The extinction conditions characteristic of the whole solid solution field are given by $F(hklm) = 0$ unless $k + l = 2n$, $F(hk0m) = 0$ unless $h = 2n$ and $F(hkl, -k) = 0$ unless $k = 2n$. The corresponding implied superspace symmetry operations are $\{E|0, \frac{1}{2}, \frac{1}{2}0\}$, $\{\sigma_z|\frac{1}{2}, 0, 0, 0\}$ and $\{\sigma_y|0, 0, 0, \frac{1}{2} - 2y\}$, respectively. The $(3+1)$-dimensional superspace group for the whole crystal and (by definition) for the metal ion subsystem is $Amma(1/x, 1, 0)0s0$ using the notation of Janssen, Janner, Looijenga-Vos & de Wolff (1992), while that

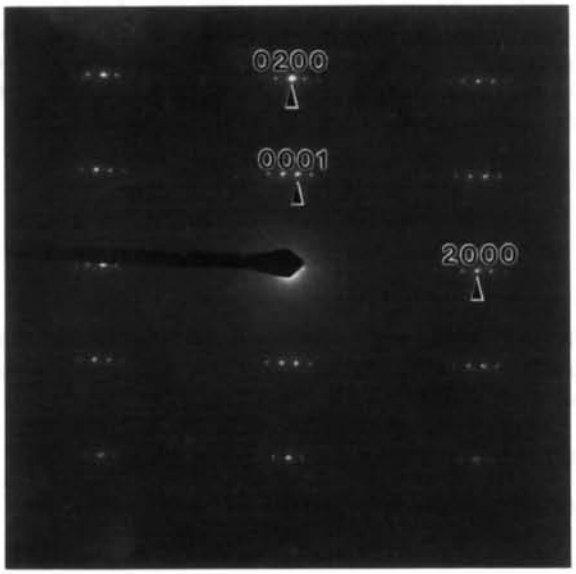

Fig. 1. Electron diffraction pattern of the $hk0$ reciprocal layer of $Nb_2Zr_{x-2}O_{2x+1}$, $x = 12$. The slightly canted rows of satellite reflections are clearly visible.

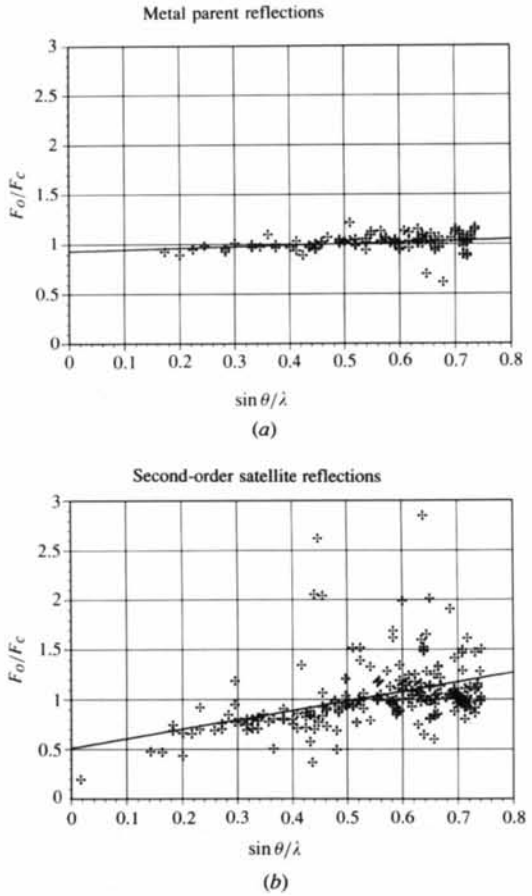

Fig. 2. Plots of F_o/F_c *versus* $\sin\theta/\lambda$ for (*a*) the metal parent and (*b*) the second-order satellite reflections of the 'far-edge' intensity data set. The linear curve represents a least-squares fit of the data to the equation $F_o/F_c = a_1(\sin\theta/\lambda) + a_2$. The coefficients a_1 and a_2 are 0.64, 0.80 and 0.96, 0.35 for the main and the satellite reflections, respectively.

for the oxygen subsystem is $Imam[x/(2x+1), 0, 0]00s$, which follows from the application of the W matrix on the symmetry operators of $Amma(1/x, 1, 0)0s0$.

(v) The origin in the fourth dimension was fixed by the superspace symmetry operation $\{i|0, 0, 0, 0\}$. This requires an origin shift of $n\mathbf{a}_O - \frac{1}{4}\mathbf{c}$ (where $n\mathbf{a}_O = p\mathbf{a}_M - \frac{1}{4}\mathbf{a}_M$, n and p integers) with respect to the origin used in WTH. [In this latter case, the relative origin of the two substructures along the **a** direction was fixed by the superspace group symmetry operation $\{\sigma_x|0, 0, 0, \frac{1}{2}\}$, which was in turn dictated by the $Ima2$ conventional superstructure space-group symmetry reported for $Nb_2Zr_6O_{17}$ (Galy & Roth, 1973).] With respect to this new origin, metal atoms of type 1 (see Fig. 2 of WTH) now occur at $\frac{1}{4}\mathbf{a}_M + (\frac{1}{4} - \delta)\mathbf{c}_M + \mathbf{T}_M$ in the parent metal substructure, whereas O atoms of type 3 (see Fig. 2 of WTH) now occur at $\frac{1}{4}\mathbf{a}_O + (\frac{1}{4} + \delta_1)\mathbf{b}_O + \frac{1}{2}\mathbf{c}_O + \mathbf{T}_O$ in the parent oxygen substructure. Here, $\mathbf{T}_M$ and $\mathbf{T}_O$ are Bravais lattice vectors of the respective parent substructures.

(vi) The above origin shift not only alters positions within each primitive parent unit cell at which atoms occur, but also the argument of the corresponding atomic modulation functions (AMF's). In the case of the metal atoms of type 1, $\mathbf{q}_M.\mathbf{T}_M$ in WTH is replaced by $\mathbf{q}_M.(\mathbf{T}_M + \frac{1}{4}\mathbf{a}_M) + \frac{1}{2}$, whereas, in the case of O atoms of type 3, $\mathbf{q}_O.(\mathbf{T}_O + \frac{1}{4}\mathbf{a}_O)$ is replaced by $\mathbf{q}_O.(\mathbf{T}_O + \frac{1}{4}\mathbf{a}_O) - \frac{1}{4}$. Thus, with respect to the new origin, the symmetry-allowed displacive AMF's are given by

$$\begin{aligned} M\text{: } \mathbf{U}_M = \mathbf{a}_M\ & \{\varepsilon_x(2\mathbf{q}_M)\sin[4\pi\mathbf{q}_M.(\mathbf{T}_M + \tfrac{1}{4}\mathbf{a}_M)] \\ & + \varepsilon_x(4\mathbf{q}_M)\sin[8\pi\mathbf{q}_M.(\mathbf{T}_M + \tfrac{1}{4}\mathbf{a}_M)]\} \\ & + \mathbf{b}\ \{-\varepsilon_y(\mathbf{q}_M)\sin[2\pi\mathbf{q}_M.(\mathbf{T}_M + \tfrac{1}{4}\mathbf{a}_M)] \\ & - \varepsilon_y(3\mathbf{q}_M)\sin[6\pi\mathbf{q}_M.(\mathbf{T}_M + \tfrac{1}{4}\mathbf{a}_M)]\} \\ & + \mathbf{c}\ \{\varepsilon_z(2\mathbf{q}_M)\cos[4\pi\mathbf{q}_M.(\mathbf{T}_M + \tfrac{1}{4}\mathbf{a}_M)] \\ & + \varepsilon_z(4\mathbf{q}_M)\cos[8\pi\mathbf{q}_M.(\mathbf{T}_M + \tfrac{1}{4}\mathbf{a}_M)]\} \end{aligned}$$

and

$$\begin{aligned} \text{O: } \mathbf{U}_O = \mathbf{a}_O\ & \{-\varepsilon_x(2\mathbf{q}_O)\sin[4\pi\mathbf{q}_O.(\mathbf{T}_O + \tfrac{1}{4}\mathbf{a}_O)] \\ & + \varepsilon_x(4\mathbf{q}_O)\sin[8\pi\mathbf{q}_O.(\mathbf{T}_O + \tfrac{1}{4}\mathbf{a}_O)]\} \\ & + \mathbf{b}\ \{-\varepsilon_y(2\mathbf{q}_O)\cos[4\pi\mathbf{q}_O.(\mathbf{T}_O + \tfrac{1}{4}\mathbf{a}_O)] \\ & + \varepsilon_y(4\mathbf{q}_O)\cos[8\pi\mathbf{q}_O.(\mathbf{T}_O + \tfrac{1}{4}\mathbf{a}_O)]\} \\ & + \mathbf{c}\ \{\varepsilon_z(\mathbf{q}_O)\sin[2\pi\mathbf{q}_O.(\mathbf{T}_O + \tfrac{1}{4}\mathbf{a}_O)] \\ & - \varepsilon_z(3\mathbf{q}_O)\sin[6\pi\mathbf{q}_O.(\mathbf{T}_O + \tfrac{1}{4}\mathbf{a}_O)]\}, \end{aligned}$$

where the **T**'s are Bravais lattice vectors and the modulation wave amplitudes correspond one-to-one with those determined for an $x = 8$ specimen in WTH. Satellite reflections up to the fourth order were taken into account for the refinement (see Tables 2 and 4). Thus, only Fourier terms up to the fourth order were included in the above displacive AMF's. The final position of the atom μ is given by $\mathbf{r}_\mu + \mathbf{T} + \mathbf{U}_\mu(\mathbf{r}_\mu + \mathbf{T})$, where $\mathbf{r}_\mu$ is the average position in the asymmetric unit of the respective parent substructure and **T** a Bravais lattice vector.

Table 4. *Relevant parameters of the refinements (resulting parameters deposited)*

(*a*)

Label of refinement run	zrf.C	zr8.C	zr8.D1	zr8.D2
Wavelength (Å)	$\lambda_2 = 0.7495$		$\lambda_1 = 0.6892$	
Energy difference to Zr K edge (eV)	1458		8	
Modulation wavevector	$\mathbf{q}_M = (1/12)\mathbf{a}_M^* + \mathbf{b}_M^*$	$\mathbf{q}_M = (1/12)\mathbf{a}_M^* + \mathbf{b}_M^*$	12-fold superstructure $I12/a1$	
	Commensurate	Commensurate		
Occupational modulation	None	None	Random ordering	Nb at site...
No. of refined parameters	26	26	1	1
No. of unique reflections $F \geq 3\sigma(F)$				
all	796	205	205	
$m = 0$	171	58		
$m = 1$	198	54		
$m = 2$	201	66		
$m = 3$	138	34		
$m = 4$	89	14		
Weight	$1/\sigma^2$	$1/\sigma^2$	$1/\sigma^2$	$1/\sigma^2$
Residuals R, wR (%)				
overall	6.81 7.25	5.29 4.53	$R_{all} = 9.91$	$R_{all} = 11.88$ ...(1)
$m = 0$	3.36 4.36	2.54 2.80		12.41 (2)
$m = 1$	11.45 10.53	11.63 9.86		11.13 (3)
$m = 2$	11.00 10.08	11.28 10.71		11.87 (4)
$m = 3$	17.10 16.28	18.31 17.22		12.42 (5)
$m = 4$	50.67 45.29	40.06 45.38		11.95 (6)

(*b*) Metal ion positions in space group $I12/a1$

Site No.	Multiplicity	x	y	z
1	8	0.0215	0.0045	0.2154
2	8	0.1063	0.0156	0.2177
3	8	0.1888	0.0122	0.2143
4	8	0.2704	0.0099	0.2121
5	8	0.3522	0.0151	0.2168
6	8	0.4359	0.0120	0.2167

(vii) Symmetry-determined constraints also apply to the coefficients of the modulation function of the thermal parameters. For the anisotropic thermal parameters of oxygen, Fourier terms up to second-order have been taken into account. Thus

$$\begin{aligned} \text{O: } u_{ii,O}(\mathbf{T}_O) &= \bar{u}_{ii} + u_{ii}(2\mathbf{q}_O)\cos[4\pi\mathbf{q}_O.(\mathbf{T}_O + \tfrac{1}{4}\mathbf{a}_O)] \\ u_{23,O}(\mathbf{T}_O) &= u_{23}(\mathbf{q}_O)\sin[2\pi\mathbf{q}_O.(\mathbf{T}_O + \tfrac{1}{4}\mathbf{a}_O)] \\ u_{13,O}(\mathbf{T}_O) &= u_{13}(2\mathbf{q}_O)\cos[4\pi\mathbf{q}_O.(\mathbf{T}_O + \tfrac{1}{4}\mathbf{a}_O)] \\ u_{12,O}(\mathbf{T}_O) &= u_{23}(2\mathbf{q}_O)\sin[4\pi\mathbf{q}_O.(\mathbf{T}_O + \tfrac{1}{4}\mathbf{a}_O)]. \end{aligned}$$

Thermal parameter modulation of the metal atom substructure was also allowed, but was subsequently found to be unrefineable (see §4).

Occupational modulation of the metal atom sites is only allowed for even-order cosine terms as follows

$$\begin{aligned} M : P_{Nb,Zr}(\mathbf{T}_M) = P_{Nb,Zr} & \\ & \pm P_{Nb,Zr}(2\mathbf{q}_M)\cos[4\pi\mathbf{q}_M.(\mathbf{T}_M + \tfrac{1}{4}\mathbf{a}_M)] \\ & \pm P_{Nb,Zr}(4\mathbf{q}_M)\cos[4\pi\mathbf{q}_M.(\mathbf{T}_M + \tfrac{1}{4}\mathbf{a}_M)], \end{aligned}$$

where the + and − signs apply to Nb and Zr,

respectively, and the average terms are set to $P_{Nb} = \frac{1}{6}$ and $P_{Zr} = \frac{5}{6}$ (*cf.* §4).

(viii) The possibility of a commensurate 12 times superstructure description was also allowed for. In general, given a certain superspace-group symmetry, the allowed three-dimensional space group depends upon the origin choice made for the so-called fourth dimension (see Yamamoto & Nakazawa, 1982; Wiegers, Meetsma, Haange, van Smaalen, de Boer, Meerschaut, Rabu & Rouxel, 1990). This corresponds in the present case to the relative positioning along the *a* direction of the *M* and O substructures at the origin. For mutually incommensurable substructures, all possible relative positionings occur at some point in the crystal and hence the choice of any particular relative positioning at the origin [*e.g.* choosing the *x*-coordinates of the *M* and O atoms in the parent substructures to be $(\frac{1}{4} + \delta_M)$ and $(\frac{1}{4} + \delta_O)$, respectively] can be made. However, when $a_O/a_M = 12/25$ exactly, the possible three-dimensional (supercell) space group is determined by the relationship between δ_M and δ_O. The allowed three-dimensional space groups can then be derived from the above superspace group and are given in the present case by

$I12/a1$ [for $\delta_O = (25/12)\delta_M + (2n/48)$, n an integer],

*Ima*2 {for $\delta_O = (25/12)\delta_M + [(2n+1)/48]$} and

$I1a1$ (otherwise).

4. Structure refinements

The refinements were carried out using the software package *JANA*94 (Petrícek, 1994). The dispersion corrections $\Delta f'$ and $\Delta f''$ for Zr and Nb were calculated using the computer program *FPRIME* of Cromer & Liberman (1981). Corrections to the relativistic part of the anomalous scattering factors were made following Kissel & Pratt (1990). Starting values for the Fourier coefficients of the displacive terms were taken from the Fourier decomposition of the structure refinement of $Nb_2Zr_6O_{17}$ (Galy & Roth, 1973; Withers *et al.*, 1991). The signs of the dominant Fourier coefficients were systematically varied and the sign combination corresponding to the true minimum was marked by a distinct drop of the residual values. In order to test the significance of the minimum found this way, the parameters were also released, setting the starting values to ±0.0001. Provided the initial sign combination was the same as previously determined, the refinement converged at the same minimum when parameters of increasing harmonic order were released successively.

The average anisotropic thermal parameters of the O atom were found to be an order of magnitude larger than those of the metal atoms. Thermal parameter modulation of the O atom substructure was refined and found to substantially improve the fit to the third- and (still more significantly) fourth-order satellite reflections. Symmetry-allowed modulation of the thermal parameters of Zr and Nb was considered to be irrelevant, after an attempt to refine the corresponding parameters failed to yield values significantly different from zero.

The scale factor was refined in the beginning and successively at later stages of the refinement using only the metal parent reflections, but was not released simultaneously with the other parameters. This would have led to a much worse fit of the main and the low-order satellite reflections in favour of the relatively weak high-order satellite reflections, owing to the chosen weighting scheme (see below). Such behaviour of the refinement could only be avoided when using unit weights.

Several weighting schemes were applied in the course of the refinement, including unit weights as well as the weighting schemes $w = 1/\sigma^2$ and $w = 1/(\sigma^2 + 0.03F^2)$. All three schemes yielded a converging refinement and led to the same resulting parameters within 6 standard deviations. However, using $w = 1/\sigma^2$ gave the best agreement between the two different intensity data sets, together with low standard deviations and a smooth distribution of the resulting residual values over the different reflection classes.

The refinements were carried out assuming **q** to be incommensurate, but the result where **q** was commensurate was also checked.

The intensity data set recorded 8 eV away from the Zr *K* absorption edge, *i.e.* at $\lambda_1 = 0.6892$ Å, was used in order to test the hypothesis that there was metal-ion ordering in $Nb_2Zr_{x-2}O_{2x+1}$. Metal-ion ordering was taken into account by allowing for occupational modulation of the metal site (see §3). The Zr:Nb ratio was assumed to be 5:1 and was not refined. This ratio was established on the basis of compositional analysis of the crystals by means of quantitative energy dispersive X-ray spectroscopic analysis, which was consistent with $x = 12$. This method, of course, does not provide a really accurate determination of the composition, but the diffraction data would not allow a reliable refinement of the Zr:Nb ratio. Furthermore, the presence of metal ion ordering was also tested, by refining the structure as a conventional 12 times superstructure, choosing as the three-dimensional space group $I12/a1$ [see §3, item (viii)]. Nb atoms were either located with full occupancy at one of the six metal positions or with $\frac{1}{6}$ occupancy on all metal sites.

5. Results and discussion

5.1. *Refinement statistics*

Table 2 displays the final agreement indices of the refinements labelled zrf.B, zr8.B1 and zr8.B2, the resulting parameters of which are presented in Tables 5 and 6. The resulting parameters of the refinements

Table 5. *Coordinates and displacive Fourier terms*

Label of refinement	zrf.B		zr8.B1		zr8.B2		Coefficient from WTH	
Zr, Nb $\frac{1}{4}$, 0, z	0.2160 (1)		0.2155 (1)		0.2157 (2)			
$\varepsilon_x(2q)$, $\varepsilon_x(4q)$	0.0237 (1)	0.0005 (3)	0.0249 (3)	0.002 (1)	0.0256 (5)	0.001 (1)	0.0244	0.0014
$\varepsilon_y(q)$, $\varepsilon_y(3q)$	−0.0158 (1)	−0.0052 (2)	−0.0159 (2)	−0.0064 (6)	−0.0160 (3)	−0.0068 (7)	−0.0185	−0.0053
$\varepsilon_z(2q)$, $\varepsilon_z(4q)$	0.0020 (1)	−0.0004 (3)	0.0017 (3)	−0.002 (1)	0.0017 (3)	−0.001 (2)	−0.0011	−0.0046
O $\frac{1}{4}$, y, $\frac{1}{2}$	0.2696 (6)		0.2699 (8)		0.2698 (8)			
$\varepsilon_x(2q)$, $\varepsilon_x(4q)$	0.198 (2)	0.061 (2)	0.191 (2)	0.058 (3)	0.192 (2)	0.058 (3)	0.1692	0.0345
$\varepsilon_y(2q)$, $\varepsilon_y(4q)$	0.0790 (9)	0.005 (1)	0.079 (1)	0.003 (2)	0.079 (1)	0.003 (2)	0.0843	−0.0007
$\varepsilon_z(q)$, $\varepsilon_z(3q)$	−0.1232 (9)	−0.0248 (9)	−0.126 (1)	−0.022 (2)	−0.126 (1)	−0.022 (1)	−0.1361	−0.0128

Table 6. *Thermal parameters and Fourier terms*

Label of refinement	zrf.B	zr8.B1	zr8.B2
Zr, Nb u_{11}	0.0095 (2)	0.0067 (6)	0.0078 (6)
u_{22}	0.0090 (2)	0.0092 (6)	0.0106 (6)
u_{33}	0.0066 (4)	0.0027 (5)	0.0041 (5)
O $\bar{u}_{11}$	0.017 (2)	0.018 (3)	0.021 (3)
$\bar{u}_{22}$	0.022 (2)	0.028 (3)	0.030 (3)
$\bar{u}_{33}$	0.025 (2)	0.026 (3)	0.028 (3)
$u_{23}(q)$	−0.005 (2)	−0.010 (3)	−0.011 (3)
$u_{13}(q)$	−0.014 (2)	−0.020 (3)	−0.020 (3)
$u_{12}(2q)$	0.015 (2)	0.017 (3)	0.017 (4)
$u_{11}(2q)$	−0.016 (3)	−0.024 (4)	−0.026 (4)
$u_{22}(2q)$	−0.006 (2)	−0.009 (4)	−0.010 (4)
$u_{33}(2q)$	−0.005 (3)	0.000 (4)	0.000 (4)

quoted in Table 4 are deposited,* because only their R-values are essential for the discussion of the results. Scan widths are shown in Table 3.

The refinement labelled zrf.B refers to the intensity data recorded 'far' from the Zr K absorption edge, while zr8.B1 and zr8.B2 refer to the data recorded 'near' (8 eV) to it. In general, all refinements converged to the same level of agreement. However, a direct comparison of the R-values of the 'far-edge' and the 'near-edge' data is rendered more difficult by the fact that the first contains almost four times as many reflections as the second one. It has to be noted that, whilst the fit for the first- and the second-order satellite reflections agrees within 1.2%, there is a discrepancy of 4.8–7.5% between the R-values of the main reflections and those of the first-order satellite reflections. This is not solely a consequence of the relative intensities of the main reflections and the satellite reflections and is discussed further in §5.5.

While the supposedly irrational part of the modulation wavevector, $\alpha\mathbf{a}_M^*$, $\alpha = 1/12$, suggests that the structure may be commensurate rather than incommensurate, the refinement assuming α to be irrational leads to distinctly lower R-values for all the classes of reflections, *cf.* the refinements zrf.C and zr8.C in Table 4 and their counterparts zrf.B and zr8.B1 in Table 2, respectively. The linear relationship between $\mathbf{q}$ and x over the compositional range investigated by Thompson *et al.* (1990), together with the better fit of the incommensurate model, are in clear favour of incommensurateness.

* A list of refinement parameters has been deposited with the IUCr (Reference: JS016). Copies may be obtained through The Managing Editor, International Union of Crystallography, 5 Abbey Square, Chester CH1 2HU, England.

5.2. *The atomic modulation functions*

The refined M and O substructure displacive AMF's are shown in Fig. 3 as a function of $\mathbf{q}_M.\mathbf{T}_M$ and $\mathbf{q}_O.\mathbf{T}_O$, respectively. The M substructure a-axis shifts are almost perfectly sinusoidal in shape, whereas those along the b axis are much more square-wave-like in appearance. The c-axis shifts, by contrast, are virtually negligible. In agreement with the known tendency to maintain the integrity of the essentially *fcc* metal-atom array, the magnitude of the metal atom shifts away from their average position remains quite small – below 0.13 Å along each basis vector direction. The absolute displacements in the O substructure, by contrast, are much larger – a maximum shift of 0.57 Å in the c-direction and displacement amplitudes of 0.56 and 0.40 Å in the a- and b-directions, respectively. The O substructure b-axis shifts are almost perfectly sinusoidal in shape, whereas those along the c axis are much more square-wave-like in appearance. The a axis AMF has some similarity to a sawtooth function.

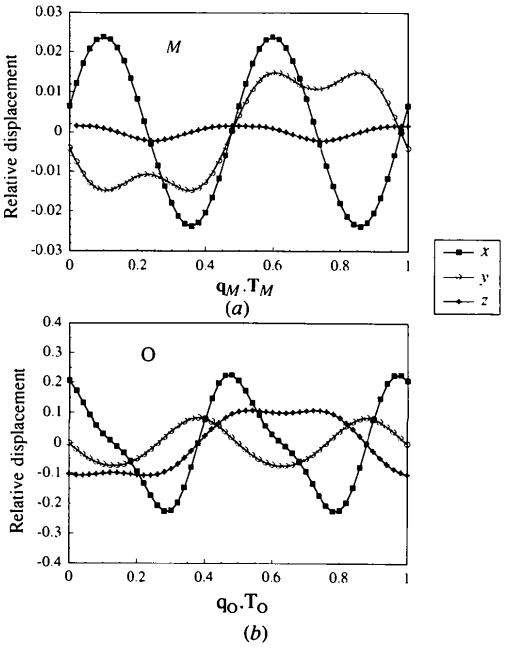

Fig. 3. Final refined (*a*) metal- and (*b*) oxygen-atom displacive atomic modulation functions plotted in fractional coordinates as a function of $\mathbf{q}_M.\mathbf{T}_M$ and $\mathbf{q}_O.\mathbf{T}_O$, respectively.

In order to compare the present structure ($x = 12$) with that of $Nb_2Zr_6O_{17}$ [$x = 8$, Galy & Roth (1973)], it is necessary to consider the Fourier decomposition reported by Withers *et al.* (1991). During the course of the present work, it was discovered that the equation $U_{O3,4}(\mathbf{T}_O) = ...$ on p. 172 of Withers *et al.* (1991) requires a sign reversal for the $\mathbf{c}_O$ term to be correct. Correspondingly, the signs of $\varepsilon_z(\mathbf{q}_O)$ and $\varepsilon_z(3\mathbf{q}_O)$ as reported in WTH have been switched and included in Table 5 for comparison with the present refinement. When this is taken into account, a comparison of the relevant Fourier coefficients, *i.e.* modulation wave amplitudes, with those of WTH (see Table 5) reveals a remarkable similarity. The displacement patterns away from the underlying parent substructures not only have the same symmetry, but the series coefficients have the same signs and their magnitudes are even quite close to each other. It can therefore be concluded that the composite crystal structures of the solid solution members $x = 8$ (Galy & Roth, 1973) and $x = 12$ (this study) of $Nb_2Zr_{x-2}O_{2x+1}$ are equivalent, not only with respect to their symmetry, but also with respect to their displacive AMF's. Thus, it appears that all crystal structures occurring in the solid solution, in principle, are equivalent.

5.3. *The coordination sphere*

Fig. 4 shows a plot of metal–oxygen distances *versus* $t' = \mathbf{q}_M.(\mathbf{T}_M - \mathbf{T}_O)$. Each curve in the plot corresponds to the distance variation of a specific metal–oxygen pair with t'. Due to the model of two interpenetrating and mutually incommensurable substructures, the relative origin of which changes continuously, the distance between a specific metal–oxygen pair goes from infinity to a minimum value and again to infinity for t' going from $-\infty$ to $+\infty$. By picking up all relevant metal–oxygen pairs in the coordination sphere of Zr and plotting them on top of each other, one obtains an intuitive picture of the variation of the metal coordination number with t'. Points in the plot, where curve intersections are situated at the same t', correspond to special sites in the superstructure. Those points occur at $t' = 11/48, 23/48$ and $35/48$, respectively.

As there is no well-defined limit for the first coordination sphere, it is not possible to decide uniquely whether an interatomic distance is, or is not, accepted as a bond. Fig. 4 shows a narrow bunch of lines between *ca* 1.95 and 2.25 Å. This suggests defining, say, 2.3 Å as an upper limit for Zr^{4+}—O^{2-} bonds. Yet a calculation of bond valence sums [or apparent valences, AV for short (Brown & Altermatt, 1985); using the program *EUTAX*1 (Brese & O'Keeffe, 1991)] shows that distances even as long as 2.6 Å still contribute to the bonding with a valence of 0.16. Within a 2.3 Å limit, the metal-atom coordination number varies between 6 and 7. Within a 2.6 Å limit, the metal-atom coordination number varies between 7 and 8.

Fig. 6(*a*) shows a section of the structure for $5/24 \leq \mathbf{q}_M.\mathbf{T}_M \leq 19/24$ projected along **c**. The sinusoidal *b*-axis O-atom shifts are clearly visible. Fig. 6(*b*) shows the same section in the projection along **b** restricting y to $0 \leq y \leq 0.05$ for clarity. The evolution of the O-atom array from a 3^6 net to a 4^4 net and back again as a function of the x coordinate is clearly visible. One can distinguish areas in Fig. 6(*a*) marked by unlinked and linked anions, with rather large and rather small displacements of the oxygens along **b**, respectively. These are associated with the 3^6 and the 4^4 net, respectively.

The nonbonded oxygen–oxygen interaction has been assumed to be of importance in limiting the Nb_2O_5-rich end of the solid solution, as the increase of the oxygen:metal ratio would eventually be limited by increasing oxygen–oxygen repulsion. This assumption is apparently supported by the rapidly decreasing a lattice parameter of the O substructure with decreasing x [$a_O(x = 12) = 2.452$, $a_O(x = 8) = 2.407$ Å]. However, considering the O—O distances for $x = 8$ and $x = 12$ (see Fig. 5), it turns out that at least the minimum O—O distance is not primarily affected by x, but is found to be essentially the same, *i.e.* ≈ 2.5 Å, for both compositions. By contrast, maximum oxygen–oxygen distances do depend strongly on x.

5.4. *Metal ordering?*

Going from $\lambda_2 = 0.7495$ Å at $\Delta E = 1458$ eV to $\lambda_1 = 0.6892$ Å at $\Delta E = 8$ eV from the ZrK absorption edge, the relative difference of the atomic scattering factors of Zr and Nb increases from *ca* 3 to 16%. This enhanced contrast should therefore allow Zr and Nb in the structure to be distinguished. The refinements zr8.B1 and zr8.B2 differ in that the former assumes a statistical distribution of the metal ions, whereas the latter allows a substitutional modulation of Zr and Nb. The slightly better residual values of zr8.B2 compared with zr8.B1 (the differences range from a few tenths of a per cent up

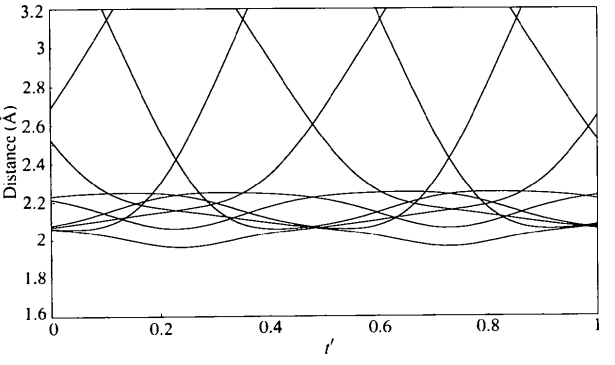

Fig. 4. Variation in the metal-ion coordination sphere as a function of $t' = \mathbf{q}_M.(\mathbf{T}_M - \mathbf{T}_O)$. Each curve represents the distance between a specific metal–oxygen pair.

to *ca* 3.5% for the fourth-order satellite reflections) seem to point to the presence of metal-ion ordering. However, the resulting values of the corresponding Fourier coefficients, describing such substitutional modulation, are $P_{Nb}(2\mathbf{q}) = -0.015(16)$ and $P_{Nb}(4\mathbf{q}) = 0.26(10)$ and thus appear to be zero within error.

The model of the conventional 12-fold superstructure was derived from the modulated structure choosing the inversion $\{\bar{1}|0,0,0,0\}$ to fix the origin in the fourth coordinate, which leads to the three-dimensional space group $I12/a1$ [see §3, item (viii)]. Three-dimensional coordinates for the superstructure were calculated from the result of refinement zr8.B1 giving six different *M*- and 13 different O-atom positions. Refining only the scale factor, distinctly lower *R*-values could be obtained when assuming a uniform distribution of Nb over the six metal sites with occupation $\frac{1}{6}$ (according to the assumed Nb:Zr ratio) rather than locating Nb on any one of the six metal-atom sites with full occupancy. Release of all the coordinates, in principle, yielded the same result, but gave rise to strong correlations between the positional parameters.

Apparent valences (Brown & Altermatt, 1985, see §5.3) calculated for the metal atom sites assuming the above coordinates were remarkably uniform. They gave no indication of a position, which might preferably be occupied by Nb. The mean AV for the metal sites with respect to $I12/a1$ is $\langle AV_M \rangle = 4.083 \pm 0.045$ with a largest deviation Δ_{max} from $\langle AV_M \rangle$ of 0.073. For the oxygens one finds $\langle AV_O \rangle = 1.960 \pm 0.023$ and $\Delta_{max} = 0.041$. The same uniformity is present when choosing the space group *Ima*2, where we have seven metal sites and the same number of oxygen sites as before. The mean AV's in this case are $\langle AV_M \rangle = 4.082 \pm 0.052$, $\Delta_{max} = 0.066$ and $\langle AV_O \rangle = 1.959 \pm 0.025$, $\Delta_{max} = 0.038$. In both cases $\langle AV_M \rangle$ is very close to 4.166, the value expected for a random distribution of Nb over the metal sites. Looking at the structure of $Nb_2Zr_6O_{17}$ and calculating AV's on the basis of the coordinates reported by Galy & Roth (1973), a larger scattering of the AV's around the mean value is observed, *i.e.* $\langle AV_M \rangle = 4.416 \pm 0.254$ and $\Delta_{max} = 0.332$, $\langle AV_O \rangle = 2.076 \pm 0.061$, $\Delta_{max} = 0.108$. However, if the AV's are based on the Fourier decomposition of WTH omitting terms higher than

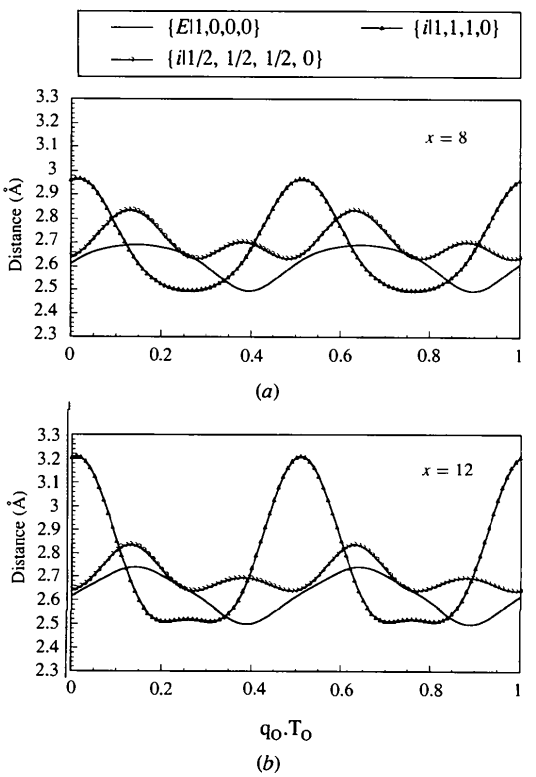

Fig. 5. Oxygen–oxygen distances as a function of $\mathbf{q}_O.\mathbf{T}_O$. The plot with $x = 8$ (*a*) has been derived from the Fourier decomposition (Withers *et al.*, 1991) of the structure refinement of $Nb_2Zr_6O_{17}$ (Galy & Roth, 1973), omitting Fourier terms higher than fourth order. The plot $x = 12$ (*b*) is derived from the refinement labelled zrf.B.

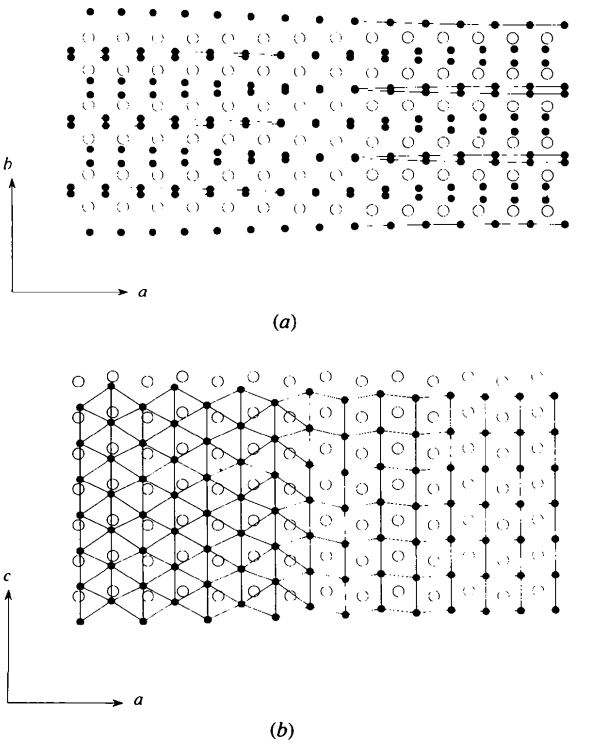

Fig. 6. (*a*) Projection of the structure of $Nb_2Zr_{x-2}O_{2x+1}$, $x = 12$, along **c** for $5/24 \leq \mathbf{q}_M.\mathbf{T}_M \leq 19/24$ and $0 \leq z \leq 1$. Open and closed circles represent metal and oxygen ions, respectively. Those oxygens linked by a solid line line are arranged as a 4^4 net [in projection along **b**, see (*b*)] and show small displacements along **b** compared with the unconnected oxygens, which are arranged in a 3^6 net (in projection along **b**). (*b*) Projection along **b** for $5/24 \leq \mathbf{q}_M.\mathbf{T}_M \leq 19/24$ and $0 \leq y \leq \frac{1}{2}$. The evolution of the O-atom array from a 3^6 net to a 4^4 net (and back again) as a function of the *x* coordinate is clearly visible.

fourth order, the scatter in AV's is substantially reduced whilst the average value is the same within a standard deviation, *i.e.* $\langle AV_M \rangle = 4.401 \pm 0.013$, and again very close to the value of 4.25 to be expected for the Zr:Nb ratio given in $Nb_2Zr_6O_{17}$.

Therefore, calculation of AV's as well as the refinement results themselves strongly suggest that there is no metal-ion ordering.

5.5. *Irrational components of* **q** *along* **b*** *and* **c***?

As mentioned in §2.3, certain electron diffraction patterns show rows of apparently quite sharp satellite reflections often slightly canted away from the $\mathbf{a}_M^*$ direction of the metal-atom substructure, implying that the irrational component of the primary modulation wavevector $\mathbf{q}_i$ need not necessarily point directly along $\mathbf{a}_M^*$. Strictly speaking, this implies that orthorhombic symmetry must be broken. The extent of the canting, however, was never reproducible and seemed to vary from grain to grain. Apparently, the local wavevector varies on a length scale smaller than the X-ray correlation length, thus giving rise to the observed substantial broadening of the satellite reflections perpendicular to, as well as along, the a^* axis. Our diffraction data are insensitive to these local perturbations, as indicated by the excellent internal R-values obtained when averaging symmetry-equivalent reflections in the Laue group *mmm* (see Table 2).

Whilst the metal ion array undergoes only relatively small amplitude atomic displacements (see §5.2), the O-atom array undergoes much larger atomic shifts (up to 0.57 Å) as well as exhibiting high average substructure thermal parameters. Similarly, whilst the parent metal substructure reflections are sharp, the parent oxygen substructure reflections are rather broad and much less well defined. We interpret these observations in terms of a rather rigid metal-ion array accompanied by an oxygen substructure, which is rather more flexible and less well determined in the sense of an ordered crystal structure. In this way, the discrepancy between the very good fit obtained for the metal parent reflections and the still acceptable but perhaps less satisfactory fit for the first- and second-order satellite reflections might become explicable. The concept of an incommensurately modulated structure, although being aperiodic in three-dimensional space, relies on the prerequisite of perfect long-range order. Such a concept is not able to account for short-range disorder without substantial modification. In fact, the behaviour of the oxygen substructure has, to a certain extent, a striking resemblance to structures for which the term '*para*-crystal' has been coined (Hosemann & Bagchi, 1962). Such a model, which accounts for short-range perturbations of the long-range structural order, combined with incommensurateness would allow for a 'wobbling' modulation wavevector and might, therefore, give a more accurate description of the crystal structure of $Nb_2Zr_{x-2}O_{2x+1}$.

6. Concluding remarks

It has been demonstrated in the present paper that the $Nb_2Zr_{x-2}O_{2x+1}$ solid solution can be described by essentially the same crystal stucture over a wide range of x, *i.e.* $x = 7.1$–12, if the concept of a modulated composite structure is applied. Long-range metal-ion ordering has been shown to be negligible and seems to be of minor importance for the understanding of the crystal structure. Whilst non-bonded oxygen–oxygen interactions are still considered to be possibly an important factor in determining the low-x, Nb_2O_5-rich end of the solid solution, the minimum O—O distance seems to be independent of x. Although the description of the $ZrO_2 + Nb_2O_5$ solid solution field in terms of a composite modulated structure is demonstrably powerful, its ability to model the structure of $Nb_2Zr_{x-2}O_{2x+1}$ may well be limited by the apparent '*para*-crystalline' behaviour of the oxygen substructure.

We would like to express our gratitude towards Dr Vaclav Petrícek for his continuing support and advise in the use of *JANA* as well as for stimulating discussions. A major part of the experimental work has been made possible by funding from the Access to Major Research Facilities fund of the Australian Federal Government and the generous allocation of beamtime (Project No. 94G136) by the National Laboratory for High Energy Physics, Tsukuba, Japan.

References

BRESE, N. E. & O'KEEFFE, M. (1991). *Acta Cryst.* B**47**, 192–197.
BROWN, I. D. & ALTERMATT, D. (1985). *Acta Cryst.* B**41**, 244–247.
CROMER, D. T. & LIBERMAN, D. A. (1981). *Acta Cryst.* A**37**, 267–268.
EYRING, L. (1979). In *Handbook on the Physics and Chemistry of the Rare Earth*, edited by K. A. GSCHNEIDNER & L. EYRING, Vol. 3, pp. 337–399. Amsterdam: North Holland.
GALY, J. (1980). Private communication.
GALY, J. & ROTH, R. S. (1973). *J. Solid State Chem.* 7, 277–285.
HALL, S. R. & STEWART, J. M. (1990). Editors. *Xtal3.0 Reference Manual*. Univs. of Western Australia, Australia, and Maryland, USA.
HOSEMANN, R. & BAGCHI, S. N. (1962). *Direct Analysis of Diffraction by Matter*. Amsterdam: North Holland.
JANSSEN, T., JANNER, A., LOOIJENGA-VOS, A. & DE WOLFF, P. M. (1992). *International Tables for Crystallography*, edited by A. J. WILSON, Vol. C, pp. 797–835, Dordrecht: Kluwer Academic Publishers.
KISSEL, L. & PRATT, R. H. (1990). *Acta Cryst.* A**46**, 170–175.
MAKOVICKY, E. & HYDE, B. G. (1981). *Struct. Bonding*, **46**, 101–176.
PETRÍCEK, V. (1994). *JANA94. Programs for Modulated and Composite Crystals*. Institute of Physics, Praha, Czech Republic.
ROTH, R. S., WARING, J. L., BROWER, W. S. & PARKER, H. S. (1972). National Bureau of Standards Special Publication 364, *Solid State Chem. Proc. 5th Mater. Res. Symp.*, pp. 183–195.
SATOW, Y. & IITAKA, Y. (1989). *Rev. Sci. Instrum.* **60**, 2390–2393.
SMAALEN, S. VAN (1991). *Phys. Rev. B*, **43**, 11330–11341.
THOMPSON, J. G., WITHERS, R. L., SELLAR, J., BARLOW, P. J. & HYDE, B. G. (1990). *J. Solid State Chem.* **88**, 465–475.
WIEGERS, G. A., MEETSMA, A., HAANGE, R. J., VAN SMAALEN, S., DE BOER, J. L., MEERSCHAUT, A., RABU, P. & ROUXEL, J. (1990). *Acta Cryst.* B**46**, 324–332.
WITHERS, R. L., THOMPSON, J. G. & HYDE, B. G. (1991). *Acta Cryst.* B**47**, 166–174.
YAMAMOTO, A. & NAKAZAWA, H. (1982). *Acta Cryst.* A**38**, 79–86.